Surface deformation of nematic elastomers under striped illumination

L. H. He*
CAS Key Laboratory of Mechanical Behavior and Design of Materials, University of Science and Technology of China, Hefei, Anhui 230026, China
(Received 8 November 2006; published 16 April 2007)

Nematic elastomers containing azobenzene chromophores are activated upon photoabsorption. We study the surface deformation of such elastomers under striped illumination. For an arbitrary orientation of the nematic axis, we obtain an analytical solution to the problem via a phenomenological continuum model. Numerical computations indicate that the profile of the deformed surface depends not only on the stripe width but also on the orientation of the nematic axis. The result may provide a mechanism to manipulate the surface topography of elastomers.

DOI: 10.1103/PhysRevE.75.041702 PACS number(s): 61.30.Vx, 83.80.Va, 46.25.Cc, 46.25.Hf

I. INTRODUCTION

Nematic elastomers can be made as large monodomains [1]. The most remarkable property of the material is that it exhibits large spontaneous contraction along the nematic axis when the degree of alignment order is changed. Typically, this can be achieved by heating through the nematic-isotropic transition temperature [2,3]. Another more novel route is by light irradiation, provided that azobenzene chromophroes are incorporated into the elastomers. In the absence of illumination, the chromophores are in the rodlike *trans* state. Light irradiation gives rise to photoisomerization of the chromophores from the *trans* to the strongly kinked cis state, thereby lowering the nematic order [4–6]. Essentially, both methods can produce the same amount of spontaneous strain, and the related thermal and optical effects can be exactly mapped onto each other [4]. A similar optical response has been found in polydomain and amorphous elastomers as well.

The unique photoelastic behavior of the nematic elastomers is especially attractive for applications in light-driven mechanical actuations [7–10]. For example, when one side of such a film is illuminated uniformly, most of the incident photons are absorbed by the surface layer of a very small thickness. The degree of photoisomerization decays rapidly with the penetration depth, thus forming a gradient of photostrain across the thickness that results in the bending of the film. Obviously, the orientation of nematic axis can strongly affect the magnitude and anisotropy of photostrains. Experiments indicate that a film with nematic axis parallel to the surface bends towards the light source, while a film with nematic axis normal to the surface bends away from it [9]. More interesting is the case of polydomain nematic elastomer films: the bending in any direction can be evoked [7]. One can optimize a film actuator made of nematic elastomers by appropriately choosing the geometry and the direction of nematic axis [11].

When the elastomers are exposed to a nonuniform illumination pattern, however, the situation becomes different. A photostrain is induced in the irradiated part but not anywhere else, leading to the formation of pits and bumps on the elastomer surface. Warner and Mahadevan [11] proposed a scaling analysis of pits and bumps induced by shining light in circular spots onto the surface of a monodomain nematic elastomer film with the nematic axis normal to the surface and suggested its use as writable structures in microfluidics, switchable reflector elements in projective displays, etc. The idea is reminiscent of the inscription of the surface relief gratings onto amorphous or liquid-crystalline polymers containing azobenzene chromophores [12–14]. Nevertheless, the microscopic scenario in the nematic elastomers is quite different, as an occasional cross-link between chains resists large-scale mass transport and elastic distortion becomes a predominant concern. Recently, Wei and He [15] performed a detailed numerical computation of the surface profile of the film analyzed by Warner and Mahadevan [11]. An interesting finding is that the photoinduced surface topography strongly depends on the radius of the light spot. The phenomenon can be attributed to elastic confinement from the less irradiated surrounding material. Consequently, in addition to illumination patterns, the distribution of elastic deformation is another influential factor for the surface profile of the elastomers.

Since the distribution of photostrain in a nematic elastomer depends on the direction of the nematic axis, the latter providing a mechanism of tailoring the field of elastic deformation. Motivated by this reason, this paper studies the effect of the orientation of the nematic axis on the photoinduced surface topography of the elastomers. For simplicity, we consider a monodomain nematic elastomer with flat surface under striped illumination of a single beam in the low pumping limit, where the orientation of the nematic axis can be arbitrary. In this circumstance, we are able to obtain an analytical steady-state solution to the surface deformation by using a phenomenological continuum model. Our analysis predicts a similar dependence of the photoinduced surface profile on the stripe width as in the case of circular light spots [15]. Moreover, we demonstrate that the orientation of the nematic axis lends itself to an adjustable parameter that can efficiently control the surface profile. The results may be used to manipulate the surface topography of azobenzene-containing nematic elastomers by nonuniform illumination.

*Corresponding author. Electronic address: lhhe@ustc.edu.cn

 ©2007 The American Physical Society

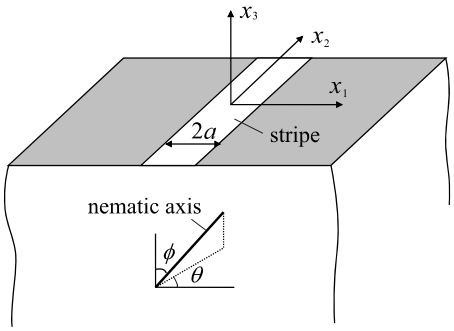

FIG. 1. Schematic illustration of the problem. A nematic elastomer is illuminated by a normally incident beam, leaving a stripe parallel to the x_2 direction on the surface. The nematic axis of the elastomer is arbitrarily aligned, it makes an angle ϕ with the x_3 direction, and its projection on the x_1-x_2 plane makes an angle θ with the x_1 direction.

II. FUNDAMENTAL FORMULATION

Monodomain nematic elastomers can be used as thin films glued onto rigid substrates, and any longitudinal deformations in the film lead to shear strains due to the restriction of the substrates [11]. When the film is sufficiently thick, photoinduced deformations in the surface region undergo a similar restriction by the less distorted underlying material [15]. Therefore, for this reason and for simplicity, we consider a semi-infinite monodomain nematic elastomer that occupies the half-space $x_3<0$, with the initially flat surface coinciding with the x_1-x_2 plane. As depicted in Fig. 1, the nematic axis of the elastomer can be along an arbitrary direction characterized by two angles θ and ϕ, where θ stands for the angle between the projection of the nematic axis on the surface and the x_1 direction, while ϕ is the angle between the nematic axis and the x_3 direction. Suppose that a light beam is incident normal to the elastomer, leaving a stripe of width $2a$ on the surface. The two parallel boundaries of the stripe are $x_1=\pm a$, respectively, and the intensity on the surface is expressed in the unified form as $I(x_1,x_2)=IH(a-|x_1|)$. Here I is a constant and $H(x)$ refers to the Heaviside function that equals unity for $x\geqslant 0$ and vanishes for $x<0$. We will study the surface deformation of the elastomer.

Before going into details, it is helpful to recall some previous results concerning photoinduced strains in a free sample of a nematic elastomer under homogeneous illumination [3–6]. Denote the number density of the azobenzene chromophores in total by ϕ_0. A homogeneous illumination of intensity I depletes the *trans* population at a rate $-\eta I(\phi_0-\phi_c)$, where η is the molecular absorption coefficient and ϕ_c the number density of the resulting *cis* isomers. The *cis* concentration increases, and then there is a back reaction to the *trans* state. The back reaction rate depends on the *cis* population and the lifetime τ_{ct}, and is expressed by ϕ_c/τ_{ct}. In the stationary state, the forward and back reactions are balanced, giving $\phi_c=\eta I\tau_{ct}\phi_0/(1+\eta I\tau_{ct})$. In the low-illumination limit $\eta I\tau_{ct}\ll 1$, one has $\phi_c=\eta I\tau_{ct}\phi_0$. Such a small amount of bent cis isomers disrupts the nematic order and leads to a spontaneous contraction proportional to ϕ_c along the nematic axis. Therefore, assuming incompressibility of the elastomer, the photostrains parallel and normal to the director axis are both uniform and read $\varepsilon_{\parallel}^*=-\alpha I$ and $\varepsilon_{\perp}^*=\alpha I/2$, respectively, where $\alpha=c\eta\tau_{ct}\phi_0$ and c is a phenomenological constant.

Clearly, the situation of the elastomer half-space under inhomogeneous illumination is much more complicated. The intensity $I(x_1,x_2,x_3)$ not only varies on the elastomer surface but also decreases with the penetration depth according to the Lambert-Beer law $I(x_1,x_2,x_3)=I(x_1,x_2)e^{x_3/d}$, in which d is the characteristic attenuation length. Thus, at an arbitrary point, the nonzero components of stationary photostrain are $\varepsilon_{\parallel}^*=-\alpha I(x_1,x_2)e^{x_3/d}$ and $\varepsilon_{\perp}^*=\alpha I(x_1,x_2)e^{x_3/d}/2$. Making use of coordinate transformation, the components of the stationary photostrain ε_{ij}^* referring to the (x_1,x_2,x_3) system are obtained as

$$\varepsilon_{ij}^*=\lambda_{ij}I(x_1,x_2)e^{x_3/d}, \tag{1}$$

where Latin indices range from 1 to 3, and λ_{ij} are given by

$$\lambda_{11}=\frac{\alpha}{2}(1-3\cos^2\theta\sin^2\phi),$$

$$\lambda_{22}=\frac{\alpha}{2}(1-3\sin^2\theta\sin^2\phi),$$

$$\lambda_{33}=\frac{\alpha}{2}(1-3\cos^2\phi),$$

$$\lambda_{12}=\lambda_{21}=-\frac{3\alpha}{2}\sin\theta\cos\theta\sin^2\phi,$$

$$\lambda_{13}=\lambda_{31}=-\frac{3\alpha}{2}\cos\theta\sin\phi\cos\phi,$$

$$\lambda_{23}=\lambda_{32}=-\frac{3\alpha}{2}\sin\theta\sin\phi\cos\phi. \tag{2}$$

The inhomogeneous photostrain is incompatible, resulting in the deformation of an irradiated element in the elastomer undergoing elastic confinement from the surrounding material. The total strain is the sum of the photostrain and the corresponding elastic strain.

Although some continuum theories have been developed for nematic elastomers [3,16,17], none of them incorporated the effect of photostrains. Only recently, Warner and Mahadevan [11] proposed a phenomenological model accounting for the photoinduced deformation of azebenzene-containing nematic elastomers. The model involves two assumptions: the deformation is small, and the nematic axis does not rotate. These are reasonable in the low-illumination limit, and the corresponding predictions can show an informative trace of real physics. Accordingly, the same assumptions will be utilized in this paper. To be general, we denote the components of displacement, strain, and stress in the elastomer by u_i, ε_{ij}, and σ_{ij}, respectively. The total strain is calculated by $\varepsilon_{ij}=(\partial u_i/\partial x_j+\partial u_j/\partial x_i)/2$, and the elastic strain is $\varepsilon_{ij}-\varepsilon_{ij}^*$. By assuming elastic isotropy and incompressibility, the constitutive law of the elastomer is written as $\sigma_{ij}=$

$-p\delta_{ij}+2\mu(\varepsilon_{ij}-\varepsilon^*_{ij})$, where $p=-\sigma_{kk}/3$ is the hydrostatic pressure, μ the shear modulus, and δ_{ij} the Kronecker delta which equals unity if $i=j$ and vanishes if $i\neq j$. Here and in the following, Einstein's summation convention is applied for repeated indices. In the absence of body force, the stress components satisfy the equilibrium equation $\partial\sigma_{ij}/\partial x_j=0$. Upon the use of the constitutive law and the incompressibility condition $\partial u_k/\partial x_k=0$, we derive from the equilibrium equation that

$$\mu\left(\frac{\partial^2 u_i}{\partial x_1^2}+\frac{\partial^2 u_i}{\partial x_2^2}+\frac{\partial^2 u_i}{\partial x_3^2}\right)-\frac{\partial p}{\partial x_i}=2\mu\frac{\partial \varepsilon^*_{ij}}{\partial x_j}. \tag{3}$$

Together with $\partial u_k/\partial x_k=0$, the above equations completely describe the steady-state deformation of the elastomer. The associated boundary conditions on the traction-free surface $x_3=0$ are $\sigma_{i3}=0$.

Since the elastomer is illuminated with the stripe parallel to the x_2 direction, its photoelastic response is independent of x_2—i.e., $u_i=u_i(x_1,x_3)$ and $p=p(x_1,x_3)$. As a consequence, Eq. (3) is reduced to

$$\mu\left(\frac{\partial^2 u_1}{\partial x_1^2}+\frac{\partial^2 u_1}{\partial x_3^2}\right)-\frac{\partial p}{\partial x_1}=2\mu\left(\frac{\partial \varepsilon^*_{11}}{\partial x_1}+\frac{\partial \varepsilon^*_{13}}{\partial x_3}\right),$$

$$\frac{\partial^2 u_2}{\partial x_1^2}+\frac{\partial^2 u_2}{\partial x_3^2}=2\left(\frac{\partial \varepsilon^*_{12}}{\partial x_1}+\frac{\partial \varepsilon^*_{23}}{\partial x_3}\right),$$

$$\mu\left(\frac{\partial^2 u_3}{\partial x_1^2}+\frac{\partial^2 u_3}{\partial x_3^2}\right)-\frac{\partial p}{\partial x_3}=2\mu\left(\frac{\partial \varepsilon^*_{13}}{\partial x_1}+\frac{\partial \varepsilon^*_{33}}{\partial x_3}\right), \tag{4}$$

and the incompressibility condition becomes

$$\frac{\partial u_1}{\partial x_1}+\frac{\partial u_3}{\partial x_3}=0. \tag{5}$$

To solve these coupled equations, the first and third equations in Eqs. (4) are differentiated with respect to x_1 and x_3, respectively. This leads to

$$\mu\left(\frac{\partial^3 u_1}{\partial x_1^3}+\frac{\partial^3 u_1}{\partial x_1\partial x_3^2}\right)-\frac{\partial^2 p}{\partial x_1^2}=2\mu\left(\frac{\partial^2 \varepsilon^*_{11}}{\partial x_1^2}+\frac{\partial^2 \varepsilon^*_{13}}{\partial x_1\partial x_3}\right),$$

$$\mu\left(\frac{\partial^3 u_3}{\partial x_1^2\partial x_3}+\frac{\partial^3 u_3}{\partial x_3^3}\right)-\frac{\partial^2 p}{\partial x_3^2}=2\mu\left(\frac{\partial^2 \varepsilon^*_{13}}{\partial x_1\partial x_3}+\frac{\partial^2 \varepsilon^*_{33}}{\partial x_3^2}\right). \tag{6}$$

In view of Eq. (5), we can replace $\partial u_3/\partial x_3$ in the second one in Eqs. (6) by $-\partial u_1/\partial x_1$. A comparison of the resulting equation with the first one in Eqs. (6) immediately gives

$$\frac{\partial^2 p}{\partial x_1^2}+\frac{\partial^2 p}{\partial x_3^2}=-2\mu\left(\frac{\partial^2 \varepsilon^*_{11}}{\partial x_1^2}+2\frac{\partial^2 \varepsilon^*_{13}}{\partial x_1\partial x_3}+\frac{\partial^2 \varepsilon^*_{33}}{\partial x_3^2}\right). \tag{7}$$

Thus, given that p is obtained from the above, the displacements u_1, u_2, and u_3 can be solved from the three equations (4) separately. In the meantime, the condition (5) provides some relations between the undetermined constants in the solutions, as will be seen in the subsequent section.

III. ANALYTICAL SOLUTION

As the deformation of the elastomer decays far away from the illuminated region, we can represent all the components of displacement, hydrostatic pressure, and photostrain by the Fourier integrals

$$u_i(x_1,x_3)=\int_{-\infty}^{\infty}\bar{u}_i(\xi,x_3)e^{i\xi x_1}\,d\xi,$$

$$p(x_1,x_3)=\int_{-\infty}^{\infty}\bar{p}(\xi,x_3)e^{i\xi x_1}\,d\xi,$$

$$\varepsilon^*_{ij}(x_1,x_3)=\int_{-\infty}^{\infty}\bar{\varepsilon}^*_{ij}(\xi,x_3)e^{i\xi x_1}\,d\xi, \tag{8}$$

in which $i=\sqrt{-1}$ and an overbar refers to the corresponding Fourier transform. For example, $\bar{\varepsilon}^*_{ij}$ is defined by

$$\bar{\varepsilon}^*_{ij}(\xi,x_3)=\frac{1}{2\pi}\int_{-\infty}^{\infty}\varepsilon^*_{ij}(x_1,x_3)e^{-i\xi x_1}\,dx_1, \tag{9}$$

which, in combination with Eq. (1), gives $\bar{\varepsilon}^*_{ij}(\xi,x_3)=\lambda_{ij}Ie^{x_3/d}\sin(a\xi)/\pi\xi$. Upon the substitution of Eqs. (8) into Eqs. (4), (5), and (7), we arrive at

$$\frac{\partial^2\bar{p}}{\partial x_3^2}-\xi^2\bar{p}=2\mu\left(\xi^2\bar{\varepsilon}^*_{11}-2i\xi\frac{\partial\bar{\varepsilon}^*_{13}}{\partial x_3}-\frac{\partial^2\bar{\varepsilon}^*_{13}}{\partial x_3^2}\right),$$

$$\mu\left(\frac{\partial^2\bar{u}_1}{\partial x_3^2}-\xi^2\bar{u}_1\right)-i\xi\bar{p}=2\mu\left(i\xi\bar{\varepsilon}^*_{11}+\frac{\partial\bar{\varepsilon}^*_{13}}{\partial x_3}\right),$$

$$\frac{\partial^2\bar{u}_2}{\partial x_3^2}-\xi^2\bar{u}_2=2\left(i\xi\bar{\varepsilon}^*_{12}+\frac{\partial\bar{\varepsilon}^*_{23}}{\partial x_3}\right),$$

$$\mu\left(\frac{\partial^2\bar{u}_3}{\partial x_3^2}-\xi^2\bar{u}_3\right)-\frac{\partial\bar{p}}{\partial x_3}=2\mu\left(i\xi\bar{\varepsilon}^*_{13}+\frac{\partial\bar{\varepsilon}^*_{33}}{\partial x_3}\right),$$

$$\frac{\partial\bar{u}_3}{\partial x_3}+i\xi\bar{u}_1=0. \tag{10}$$

The solutions to the above ordinary differential equations can be obtained as

$$\bar{u}_1=c_1e^{|\xi|x_3}-ic_4\frac{1-2|\xi|x_3}{4\mu\xi}e^{|\xi|x_3}+\frac{2Id[\lambda_{13}(1+d^2\xi^2)+i(\lambda_{11}-\lambda_{33})d\xi]}{\pi\xi(1-d^2\xi^2)^2}e^{x_3/d}\sin(a\xi),$$

$$\bar{u}_2=c_2e^{|\xi|x_3}+\frac{2Id(\lambda_{23}+i\lambda_{12}d\xi)}{\pi\xi(1-d^2\xi^2)}e^{x_3/d}\sin(a\xi),$$

$$\bar{u}_3=c_3e^{|\xi|x_3}-c_4\frac{1-2|\xi|x_3}{4\mu|\xi|}e^{|\xi|x_3}-\frac{2Id^2[i\lambda_{13}(1+d^2\xi^2)-(\lambda_{11}-\lambda_{33})d\xi]}{\pi\xi(1-d^2\xi^2)^2}e^{x_3/d}\sin(a\xi),$$

$$\bar{p} = c_4 e^{|\xi|x_3} - \frac{2\mu I(\lambda_{33} + 2i\lambda_{13}d\xi - \lambda_{11}d^2\xi^2)}{\pi\xi(1 - d^2\xi^2)} e^{x_3/d} \sin(a\xi), \tag{11}$$

where $c_4 = -2\mu(i\xi c_1 + |\xi| c_3)$ and c_1, c_2, and c_3 are yet unknown constants. Note that the relation between c_1, c_3, and c_4 has been derived by inserting Eqs. (11) into Eq. (5). To determine the unknown constants, we apply Fourier integral transforms to the surface boundary conditions and invoke the constitutive law. This results in $\partial\bar{u}_1/\partial x_3 + i\xi\bar{u}_3 - 2\bar{\varepsilon}^*_{13} = 0$, $\partial\bar{u}_2/\partial x_3 - 2\bar{\varepsilon}^*_{23} = 0$, and $2\mu(\partial\bar{u}_3/\partial x_3 - \bar{\varepsilon}^*_{33}) - \bar{p} = 0$ at $x_3 = 0$. Substitution of Eqs. (11) into these relations yields

$$c_1 = -\frac{dI(3 - d|\xi|)[i(\lambda_{11} - \lambda_{33})(1 + d^2\xi^2) + 4\lambda_{13}d\xi]\sin(a\xi)}{2\pi|\xi|(1 - d^2\xi^2)^2},$$

$$c_2 = -\frac{2dI(i\lambda_{12} + \lambda_{23}d\xi)\sin(a\xi)}{\pi|\xi|(1 - d^2\xi^2)},$$

$$c_3 = -\frac{dI(1 + d|\xi|)[(\lambda_{11} - \lambda_{33})(1 + d^2\xi^2) - 4i\lambda_{13}d\xi]\sin(a\xi)}{2\pi\xi(1 - d^2\xi^2)^2}. \tag{12}$$

With the results in Eqs. (11) and (12), the displacement components of the elastomer are determined in integral forms as in Eqs. (8). In particular the surface displacement field is expressed by

$$u_1(x_1,0) = \frac{dI}{\pi}\int_{-\infty}^{\infty} \frac{[2\lambda_{13} - i(\lambda_{11} - \lambda_{33})\mathrm{sgn}(t)]\sin(rt)}{t(1 + |t|)^2} e^{i\rho t}\, dt,$$

$$u_2(x_1,0) = \frac{2dI}{\pi}\int_{-\infty}^{\infty} \frac{[\lambda_{23} - i\lambda_{12}\,\mathrm{sgn}(t)]\sin(rt)}{t(1 + |t|)} e^{i\rho t}\, dt,$$

$$u_3(x_1,0) = -\frac{dI}{\pi}\int_{-\infty}^{\infty} \frac{[(\lambda_{11} - \lambda_{33})\mathrm{sgn}(t) + 2i\lambda_{13}]\sin(rt)}{(1 + |t|)^2} e^{i\rho t}\, dt, \tag{13}$$

in which t, r, and ρ are dimensionless parameters defined by

$$t = d\xi, \quad r = \frac{a}{d}, \quad \rho = \frac{x_1}{d}. \tag{14}$$

Obviously, the expression of $u_1(x_1,0)$ in Eqs. (13) can be rewritten as

$$u_1(x_1,0) = \frac{dI}{\pi}\left\{\int_{-\infty}^{0} \frac{[2\lambda_{13} + i(\lambda_{11} - \lambda_{33})]\sin(rt)e^{i\rho t}}{t(1 - t)^2} dt + \int_{0}^{\infty} \frac{[2\lambda_{13} - i(\lambda_{11} - \lambda_{33})]\sin(rt)e^{i\rho t}}{t(1 + t)^2} dt\right\}. \tag{15}$$

By taking a transformation $t \to -t$ for the first integral and then performing a simple algebraic manipulation, it is obtained that

$$u_1(x_1,0) = \frac{2dI}{\pi}\{(\lambda_{11} - \lambda_{33})[I_1(\rho) - I_3(\rho)] + 2\lambda_{13}[I_2(\rho) - I_4(\rho)]\}. \tag{16}$$

Applying similar procedures to the expressions of $u_2(x_1,0)$ and $u_3(x_1,0)$ in Eqs. (13) leads to

$$u_2(x_1,0) = \frac{4dI}{\pi}[\lambda_{12}I_1(\rho) + \lambda_{23}I_2(\rho)],$$

$$u_3(x_1,0) = \frac{2dI}{\pi}[2\lambda_{13}I_3(\rho) - (\lambda_{11} - \lambda_{33})I_4(\rho)]. \tag{17}$$

In Eqs. (16) and (17), the functions $I_1(\rho)$, $I_2(\rho)$, $I_3(\rho)$, and $I_4(\rho)$ are defined by

$$I_1(\rho) = \int_0^{\infty} \frac{\sin(\rho t)\sin(rt)}{t(1 + t)} dt,$$

$$I_2(\rho) = \int_0^{\infty} \frac{\cos(\rho t)\sin(rt)}{t(1 + t)} dt,$$

$$I_3(\rho) = \int_0^{\infty} \frac{\sin(\rho t)\sin(rt)}{(1 + t)^2} dt,$$

$$I_4(\rho) = \int_0^{\infty} \frac{\cos(\rho t)\sin(rt)}{(1 + t)^2} dt. \tag{18}$$

To evaluate these integrals, two cases have to be distinguished—i.e., $\rho \neq \pm r$ and $\rho = \pm r$. For $\rho \neq \pm r$, we can infer from Eqs. (18) that

$$I_1(\rho) = \int_0^{\infty} \frac{\sin(\rho t)\sin(rt)}{t} dt - \frac{1}{2}\int_0^{\infty} \frac{\cos(\rho - r)t}{1 + t} dt + \frac{1}{2}\int_0^{\infty} \frac{\cos(\rho + r)t}{1 + t} dt,$$

$$I_2(\rho) = \frac{1}{2}\int_0^{\infty} \frac{\sin(\rho + r)t}{t(1 + t)} dt - \frac{1}{2}\int_0^{\infty} \frac{\sin(\rho - r)t}{t(1 + t)} dt,$$

$$I_3(\rho) = \frac{1}{2}\int_0^{\infty} \frac{\cos(\rho - r)t}{(1 + t)^2} dt - \frac{1}{2}\int_0^{\infty} \frac{\cos(\rho + r)t}{(1 + t)^2} dt,$$

$$I_4(\rho) = \frac{1}{2}\int_0^{\infty} \frac{\sin(\rho + r)t}{(1 + t)^2} dt - \frac{1}{2}\int_0^{\infty} \frac{\sin(\rho - r)t}{(1 + t)^2} dt. \tag{19}$$

All the integrals in the above equation are convergent and can be represented in terms of some special functions [18]. The results are

$$I_1(\rho) = \frac{1}{2}\ln\left|\frac{\rho + r}{\rho - r}\right| + \frac{1}{4\sqrt{\pi}}\left[G^{3,1}_{1,3}\left(\frac{|\rho + r|}{2}, \frac{1}{2}\middle|{}^{0}_{0,0,1/2}\right) - G^{3,1}_{1,3}\left(\frac{|\rho - r|}{2}, \frac{1}{2}\middle|{}^{0}_{0,0,1/2}\right)\right],$$

$$I_2(\rho)=\frac{\pi}{4}\{[1-\cos(\rho+r)]\mathrm{sgn}(\rho+r)-[1-\cos(\rho-r)]\mathrm{sgn}(\rho-r)\}-\frac{1}{2}[\mathrm{Ci}(|\rho+r|)\sin(\rho+r)-\mathrm{Ci}(|\rho-r|)\sin(\rho-r)]+\frac{1}{2}[\mathrm{Si}(\rho+r)\cos(\rho+r)-\mathrm{Si}(\rho-r)\cos(\rho-r)],$$

$$I_3(\rho)=\frac{1}{2\sqrt{\pi}}\left[G_{1,3}^{3,1}\left(\frac{|\rho-r|}{2},\frac{1}{2}\middle|\begin{matrix}0\\0,1/2,1\end{matrix}\right)-G_{1,3}^{3,1}\left(\frac{|\rho+r|}{2},\frac{1}{2}\middle|\begin{matrix}0\\0,1/2,1\end{matrix}\right)\right],$$

$$I_4(\rho)=\frac{1}{2\sqrt{\pi}}\left[G_{1,3}^{3,1}\left(\frac{|\rho+r|}{2},\frac{1}{2}\middle|\begin{matrix}1/2\\1/2,1/2,1\end{matrix}\right)\mathrm{sgn}(\rho+r)-G_{1,3}^{3,1}\left(\frac{|\rho-r|}{2},\frac{1}{2}\middle|\begin{matrix}1/2\\1/2,1/2,1\end{matrix}\right)\mathrm{sgn}(\rho-r)\right]. \quad (20)$$

Here $\mathrm{sgn}(x)$ is the sign function, $\mathrm{Si}(x)$ and $\mathrm{Ci}(x)$ are, respectively, the sine and cosine integral functions defined by

$$\mathrm{Si}(x)=\int_0^x\frac{\sin t}{t}dt,\quad \mathrm{Ci}(x)=-\int_x^\infty\frac{\cos t}{t}dt, \quad (21)$$

and $G_{p,q}^{m,n}(x,r|_{b_1,\ldots,b_q}^{a_1,\ldots,a_p})$ is the Meijer G function [19] defined by

$$G_{p,q}^{m,n}(x,r|_{b_1,\ldots,b_q}^{a_1,\ldots,a_p})=\frac{1}{2\pi i}\times\int_{\gamma_1}\frac{\prod_{j=1}^{m}\Gamma(b_j+s)\prod_{j}^{n}\Gamma(1-a_j-s)}{\prod_{j=n+1}^{p}\Gamma(a_j+s)\prod_{j=m+1}^{q}\Gamma(1-b_j-s)}x^{-s/r}ds, \quad (22)$$

where $i=\sqrt{-1}$, $\Gamma(z)$ is the gamma function, and the contour γ_1 is set up between the poles of $\Gamma(1-a_j-s)$ and the poles of $\Gamma(b_j+s)$.

For $\rho=\pm r$, however, the integrals in the expression of $I_1(\rho)$ given by Eqs. (19) do not converge. To estimate $I_1(\rho)$, we can use its original definition in Eqs. (18) directly. The result is known [18] and reads

$$I_1(\rho)=\frac{1}{2}\left\{\gamma+\ln 2r+\left[\frac{\pi}{2}-\mathrm{Si}(2r)\right]\sin 2r+\mathrm{Ci}(2r)\cos 2r\right\}\mathrm{sgn}(\rho). \quad (23)$$

In contrast, there are no such problems of convergency for $I_2(\rho)$, $I_3(\rho)$, and $I_4(\rho)$ in Eqs. (19). But due to $\rho=\pm r$, the corresponding expressions are simplified to

$$I_2(\rho)=\frac{\pi}{2}\sin^2 r+\frac{1}{2}[\mathrm{Si}(2r)\cos 2r-\mathrm{Ci}(2r)\sin(2r)],$$

$$I_3(\rho)=\frac{1}{2}\left[1-\frac{1}{\sqrt{\pi}}G_{1,3}^{3,1}(r^2|_{0,1/2,1}^{0})\right]\mathrm{sgn}(\rho),$$

$$I_4(\rho)=\frac{1}{2\sqrt{\pi}}G_{1,3}^{3,1}(r^2|_{1/2,1/2,1}^{1/2}). \quad (24)$$

IV. RESULTS AND DISCUSSIONS

The solution obtained in the preceding section enables us to analyze in detail the influences of such factors as stripe width and nematic axis direction on the photoinduced surface deformation of the elastomer. In the following, we will discuss first two special cases of $\phi=\pi/2$ and $\phi=0$ and then the more general case of $0<\phi<\pi/2$. For convenience, the surface displacement components are normalized as

$$U_1=\frac{\pi}{\alpha dI}u_1(x_1,0),\quad U_2=\frac{\pi}{\alpha dI}u_2(x_1,0),\quad U_3=\frac{\pi}{\alpha dI}u_3(x_1,0). \quad (25)$$

A. Case of $\phi=\pi/2$

When the nematic axis of the elastomer is aligned parallel to the surface, making an arbitrary angle θ with the x_1 direction, we have $\phi=\pi/2$. Then the nonzero components of λ_{ij} are $\lambda_{11}=\alpha(1-3\cos^2\theta)/2$, $\lambda_{22}=\alpha(1-3\sin^2\theta)/2$, $\lambda_{33}=\alpha/2$, and $\lambda_{12}=-3\alpha\sin\theta\cos\theta/2$, and the normalized surface displacement components become

$$U_1=-3[I_1(\rho)-I_3(\rho)]\cos^2\theta,$$

$$U_2=-3I_1(\rho)\sin 2\theta,$$

$$U_3=3I_4(\rho)\cos^2\theta. \quad (26)$$

Clearly, they depend on the angle θ. At a given position ρ on the surface, the magnitudes of both U_1 and U_3 attain the

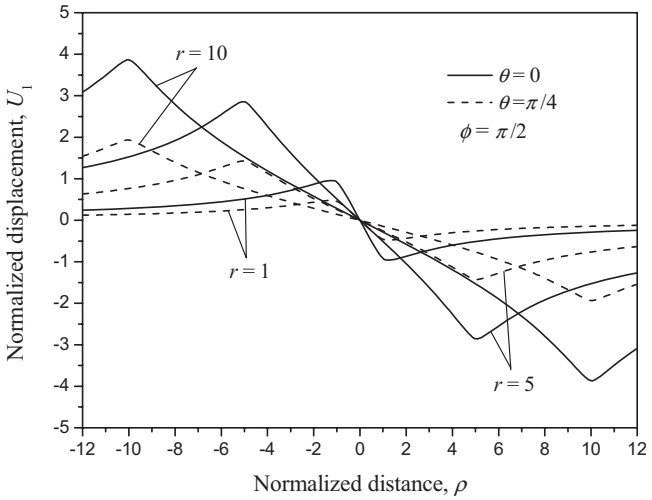

FIG. 2. Distributions of the normalized displacement U_1 at different values of normalized stripe width r, where the nematic axis may have two orientations: $\phi=\pi/2$ and $\theta=0$ or $\phi=\pi/2$ and $\theta=\pi/4$.

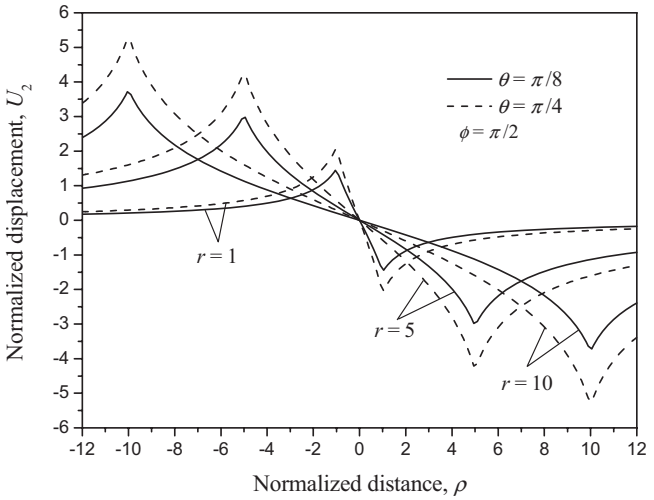

FIG. 3. Distributions of the normalized displacement U_2 at different values of normalized stripe width r, where the nematic axis may have two orientations: $\phi=\pi/2$ and $\theta=\pi/8$ or $\phi=\pi/2$ and $\theta=\pi/4$.

maximum when $\theta=0$ or π, while that of U_2 takes the maximum when $\theta=\pm\pi/4$. If $\theta=\pm\pi/2$, all the displacement components vanish, because the photoinduced contraction of the elastomer in the x_2 direction is fully constrained.

Figures 2 and 3 illustrate variations of U_1 and U_2, respectively, in and around the illuminated regions with $r=1$, 5, and 10 for some typical values of θ. As expected, the displacement components exhibit antisymmetric distributions about the x_2-x_3 plane and depend not only on the angle θ but also on the normalized stripe width r. For fixed θ and r, the magnitudes of U_1 and U_2 increase with the dimensionless distance ρ increasing from the stripe center, attain the maximum at the two boundaries $\rho=\pm r$, and then experience a sharp transition to decrease. Varying θ and r leads to changes in the magnitudes of U_1 and U_2, but does not alter the fundamental feature of the displacement distributions. At a

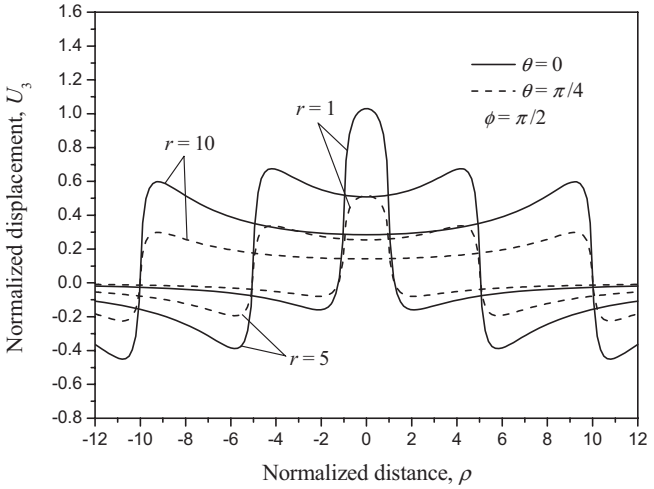

FIG. 4. Distributions of the normalized displacement U_3 at different values of normalized stripe width r, where the nematic axis may have two orientations: $\phi=\pi/2$ and $\theta=0$ or $\phi=\pi/2$ and $\theta=\pi/4$.

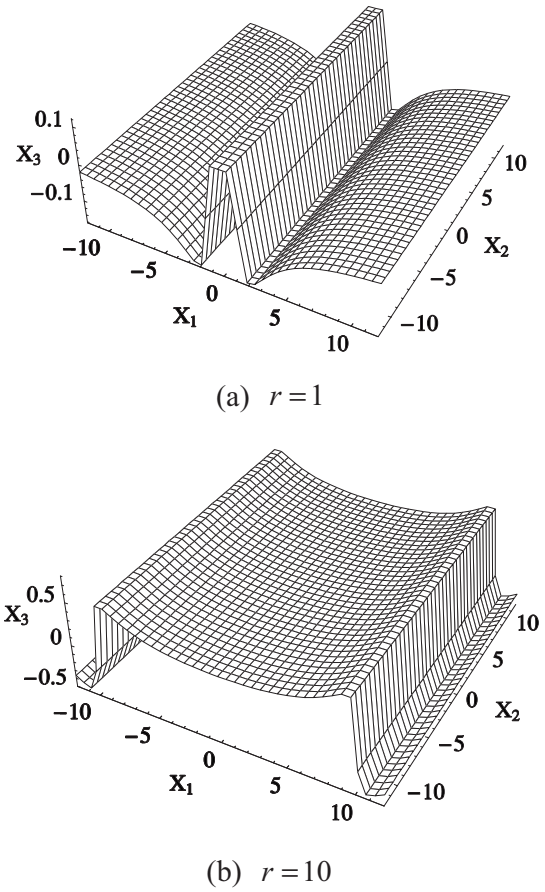

FIG. 5. Surface topographies for two normalized stripe widths: (a) $r=1$ and (b) $r=10$, where the orientation of the nematic axis is given by $\phi=\pi/2$ and $\theta=0$. The scales in the three directions are normalized by $X_1=x_1/d$, $X_2=x_2/d$, and $X_3=\pi x_3/\alpha dI$, respectively.

given angle θ, the maximal displacements, appearing at $\rho=\pm r$, are considerably dependent on the normalized stripe width r. Depicted in Fig. 4 are the variations of U_3 for $r=1$, 5, and 10. All the results are symmetric about the x_2-x_3 plane. In contrast to the cases of U_1 and U_2, the distribution of U_3 changes qualitatively for different values of the stripe width r. For example, for $r=1$, U_3 is maximal at the center ($\rho=0$) of the stripe, while for $r=5$ and 10, it attains the maximum at the positions closely near the stripe boundaries ($\rho=\pm r$).

The surface topography of the elastomer after deformation is described by the position vector $\mathbf{r}=[x_i+u_i(x_1,0)]\mathbf{e}_i$, where $\mathbf{e}_i$ stands for the base vector of x_i. In the low-illumination limit considered here, due to $\alpha I/\pi \ll 1$, it can be verified that the position vector is nearly the same as $\mathbf{r}=x_1\mathbf{e}_1+x_2\mathbf{e}_2+u_3(x_1,0)\mathbf{e}_3$. Thus, according to Eqs. (25), we can plot normalized three-dimensional profiles of the deformed surface under different conditions. Shown in Figs. 5(a) and 5(b) are two typical results for $r=1$ and 10, respectively, where $\theta=0$ is taken. For $r=1$, a single ridge forms on the surface, while for $r=10$, an M-shaped profile of the surface appears. This transition of surface topography can be explained analogously by elastic confinement as for the case of shining a beam in circular spots onto an elastomer with its nematic axis normal to the surface [15]. In fact, when the

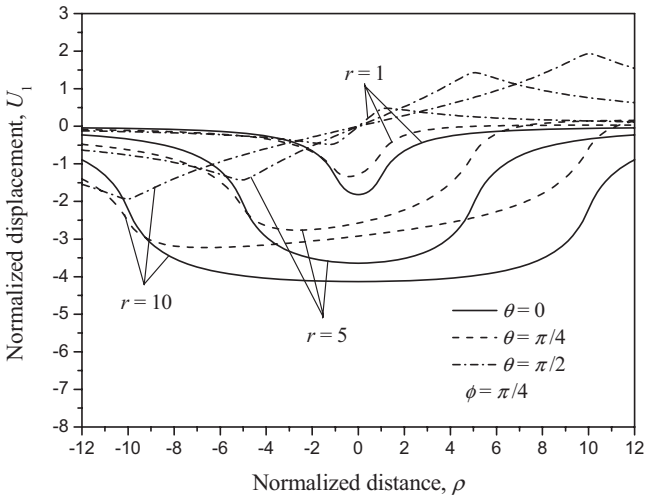

FIG. 6. Distributions of the normalized displacement U_1 at different values of normalized stripe width r, where the nematic axis may have three orientations: $\phi=\pi/4$ and $\theta=0$, $\phi=\pi/4$ and $\theta=\pi/4$, or $\phi=\pi/4$ and $\theta=\pi/2$.

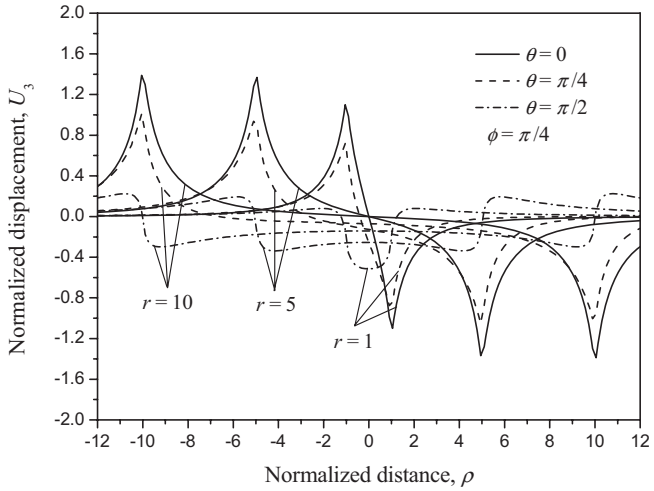

FIG. 8. Distributions of the normalized displacement U_3 at different values of normalized stripe width r, where the nematic axis may have three orientations: $\phi=\pi/4$ and $\theta=0$, $\phi=\pi/4$ and $\theta=\pi/4$, or $\phi=\pi/4$ and $\theta=\pi/2$.

stripe width is very small, the contraction of the irradiated elastomer along the nematic axis bears resistance, mainly from the unexposed material near the stripe boundaries. As a consequence of the incompressibility, the illuminated elastomer protrudes while the unexposed material near the stripe boundaries caves in, just as the case in Fig. 5(a). When the stripe width is very large, however, the contraction undergoes an additional resistance from the underlying less deformed material. Accordingly, the actual contraction is significantly smaller in the central part than near the stripe boundaries. Therefore, the illuminated part of the elastomer protrudes more in the boundary region than at the center, forming a centrally concave surface topography shown in Fig. 5(b). This interpretation is consistent with the distribution of U_1 in Fig. 2. We can see that the strain component ε_{11} is compressive and tensile in and out of the illuminated part,

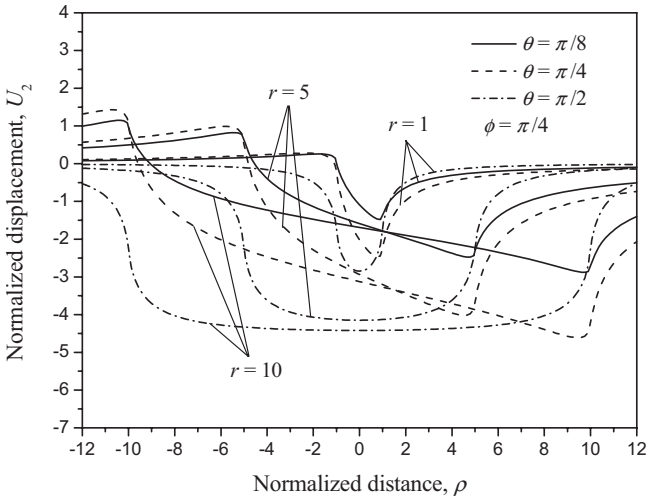

FIG. 7. Distributions of the normalized displacement U_2 at different values of normalized stripe width r, where the nematic axis may have three orientations: $\phi=\pi/4$ and $\theta=\pi/8$, $\phi=\pi/4$ and $\theta=\pi/4$, or $\phi=\pi/4$ and $\theta=\pi/2$.

respectively. For a small value of r, the compressive strain in the illuminated material is nearly constant; for a large value of r, the strain is smaller at the center than in the region near the stripe boundaries.

B. Case of $\phi=0$

When the nematic axis is aligned normal to the surface, we have $\phi=0$. In this situation the nonzero components of λ_{ij} read $\lambda_{11}=\lambda_{22}=1/2$ and $\lambda_{33}=-1$, and the normalized surface displacement components are reduced to

$$U_1 = 3[I_1(\rho) - I_3(\rho)],$$

$$U_2 = 0,$$

$$U_3 = -3I_4(\rho). \tag{27}$$

It is interesting that these expressions are attainable directly from Eqs. (26) by taking $\theta=0$ and then adding a minus sign in front of the result. For any value of the normalized stripe width r, the corresponding surface topography is a mirror reflection of that described by Eqs. (26) with $\theta=0$.

Detailed plots of the surface profiles are not given here. Instead, we provide a brief explanation for the above phenomenon as follows. Imagine that an infinitesimal cuboid with sides parallel to the coordinate axes is isolated from the irradiated part of the elastomer. The light intensity within such a small element is essentially homogeneous. If the nematic axis is along the x_1 direction—i.e., $\theta=0$—a contractible photostrain $-\varepsilon^*$ is produced in the same direction. Since no deformation in the x_2 direction is allowed, incompressibility of the elastomer leads to an effective expansive strain ε^* in the x_3 direction. The reasoning applies equally to the situation if the nematic axis is normal to the surface: a contractible photostrain $-\varepsilon^*$ in the x_3 direction causes an effective expansion ε^* along the x_1 axis. Therefore, the normalized deformations for both alignments of nematic axis are of the same magnitude but opposite signs.

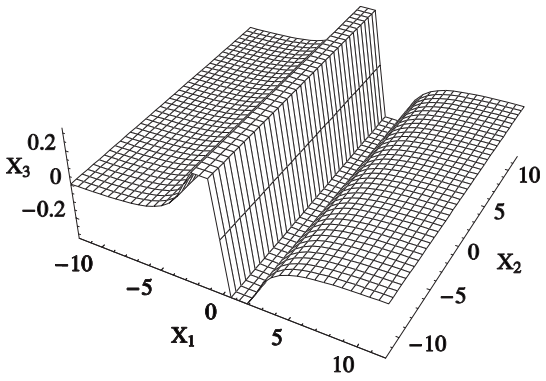

(a) $r=1$

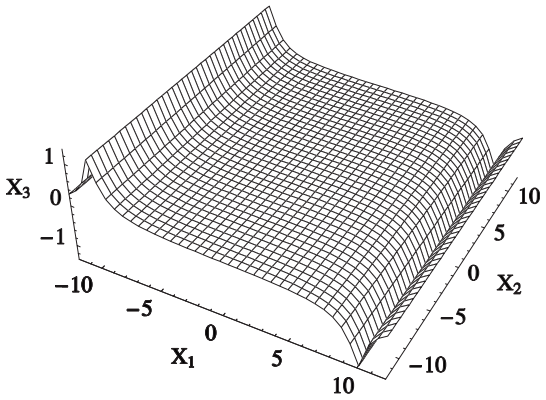

(b) $r=10$

FIG. 9. Surface topographies for two normalized stripe widths: (a) $r=1$ and (b) $r=10$, where the orientation of the nematic axis is given by $\phi=\pi/4$ and $\theta=0$. The scales in the three directions are normalized by $X_1=x_1/d$, $X_2=x_2/d$, and $X_3=\pi x_3/\alpha dI$, respectively.

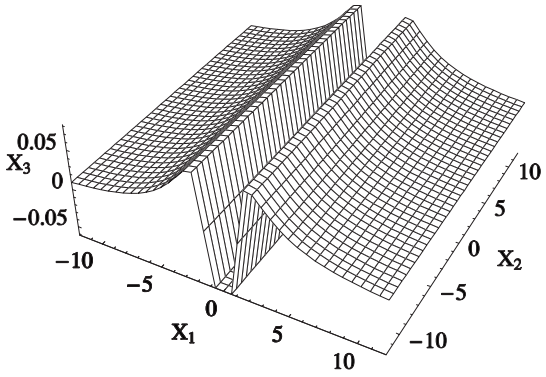

(a) $r=1$

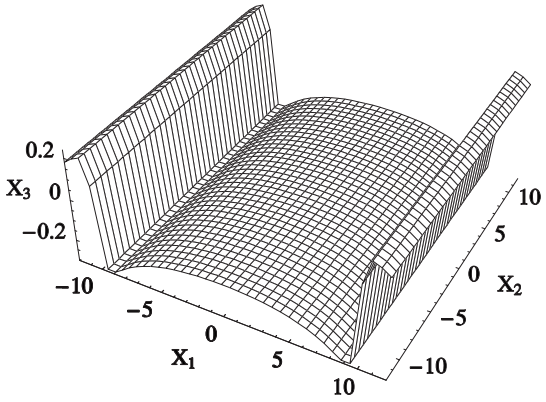

(b) $r=10$

FIG. 10. Surface topographies for two normalized stripe widths: (a) $r=1$ and (b) $r=10$, where the orientation of the nematic axis is given by $\phi=\pi/4$ and $\theta=\pi/2$. The scales in the three directions are normalized by $X_1=x_1/d$, $X_2=x_2/d$, and $X_3=\pi x_3/\alpha dI$, respectively.

C. Case of $0<\phi<\pi/2$

In the general situation of $0<\phi<\pi/2$, the nematic axis is neither parallel nor normal to the surface. The surface displacement components are more complicated and are described by the full set of equations (16) and (17). Since $I_2(\rho)$ and $I_4(\rho)$ are symmetric while $I_1(\rho)$ and $I_3(\rho)$ are antisymmetric about the normalized distance ρ, we know that each of $u_1(x_1,0)$, $u_2(x_1,0)$, and $u_3(x_1,0)$ is composed of a symmetric and an antisymmetric part. Then, adjusting the three independent parameters ϕ, θ, and r can lead to diverse surface profiles of the elastomer: symmetric, antisymmetric, and asymmetric. We have examined numerically the influence of the angle ϕ and found that a change in ϕ only leads to quantitative variation of the surface profile. In contrast, the effect of the angle θ on the surface topography may be qualitative. Thus, without loss of generality, $\phi=\pi/4$ is always assumed in the following discussions.

Plotted in Fig. 6 are the variations of U_1 for stripe widths $r=1$, 5, and 10. For $\theta=0$, the distribution of U_1 is symmetric about the x_2-x_3 plane as its antisymmetric part disappears due to $\lambda_{11}-\lambda_{33}=0$. However, this is not the case when ϕ takes values other than $\pi/4$. For $\theta=\pi/4$, U_1 distributes asymmetrically. For $\theta=\pi/2$, the symmetric nature of the molecular arrangement in the elastomer dictates $\lambda_{13}=0$ and hence the antisymmetric distribution of U_1 about ρ. Demonstrated in Fig. 7 are the variations of U_2 for $r=1$, 5, and 10. Because $U_2=0$ at $\theta=0$, the results for $\theta=\pi/8$, $\pi/4$, and $\pi/2$ are given there. Obviously, U_2 exhibits asymmetric distributions for both $\theta=\pi/8$ and $\pi/4$, but still possesses a symmetric character for $\theta=\pi/2$ in view of the molecular arrangement that results in $\lambda_{12}=0$. The variations of U_3 for $r=1$, 5, and 10 are depicted in Fig. 8, where θ takes the values of 0, $\pi/4$, and $\pi/2$. The distribution of U_3 at $\theta=0$ is antisymmetric as $\lambda_{11}-\lambda_{33}=0$, while symmetric at $\theta=\pi/2$ due to $\lambda_{13}=0$. At the intermediate value of $\theta=\pi/4$, U_3 is neither symmetric nor strictly antisymmetric distributed because λ_{13} and $\lambda_{11}-\lambda_{33}$ do not vanish in this case.

With the expressions of the displacement components, we can construct the three-dimensional topography of the deformed surface as well. Again, for the reason of $\alpha I/\pi \ll 1$, the normalized profile of the surface is nearly the same as that of U_3. Figures 9(a) and 9(b) show the surface topographies for $\phi=\pi/4$ and $\theta=0$ at $r=1$ and 10, respectively. Each figure combines a ridge and a valley in an antisymmetric pattern, forming a cross section like the letter "N." Increasing the stripe width r, the ridge and the valley separate far

away. Figures 10(a) and 10(b) illustrate the surface topographies for $\phi=\pi/4$ and $\theta=\pi/2$ at $r=1$ and 10, respectively. Different from the case of $\theta=0$, the surface profiles now become symmetric. For the small stripe width of $r=1$, the cross section of the surface profile has the shape of the letter "V," while for the large stripe width of $r=10$ the cross section resembles the letter "W." The scenario is much like that in the case when the nematic axis of the elastomer is aligned normal to the surface—i.e. $\phi=0$. The transition of surface topography between the "V" and "W" shapes can be interpreted analogously by elastic confinement from the less deformed underneath material, as elucidated previously for the case of $\phi=\pi/2$.

V. CONCLUSIONS

Surface deformation of azobenzene-containing nematic elastomers induced by a single beam in striped illumination is studied. The orientation of the nematic axis is arbitrary, but the elastic anisotropy of the elastomer is neglected. In addition, only the low-illumination limit is considered, so that the deformation is small. Using a phenomenological continuum model, we obtain an analytical solution to the steady-state surface displacement components. The result enables us to analyze in detail the effect of such factors as the width of the stripe and the orientation of the nematic axis on the surface deformation profile. Indeed, even for the relatively simple case of a single beam in striped illumination, our work predicts rich surface topographies provided that the orientations of the nematic axis and the stripe width are properly tailored. We thus expect that inhomogeneous illumination can be used as an efficient way to manipulate the surface topography of the nematic elastomers.

In practical applications, one may design diverse illumination patterns by using photomasks so as to produce much more complicated surface features. But sometimes a pattern cannot be simply duplicated onto the elastomer surface because a topographical transition may occur due to elastic confinement when the pattern size is varied, as elucidated in the present analysis. Moreover, at higher light intensity, the relationship between photostrain and intensity is nonlinear [20], and large deformation of the elastomer may lead to elastic buckling in some locations. These issues, along with the effect of elastic anisotropy of the elastomer, remain to be understood thoroughly. Exploration of the problems will be the main content in our future study.

ACKNOWLEDGMENTS

This work is supported by the Chinese National Natural Science Foundation (Grants Nos. 10472109 and 10625212), the Basic Research Program of China (Grant. No. 2006CB300404), and the Ministry of Education of China (Grant No. 20060358044).

[1] J. Küpfer and H. Finkelmann, Makromol. Chem., Rapid Commun. **12**, 717 (1991).
[2] N. Assfalg and H. Finkelmann, Kautsch. Gummi Kunstst. **52**, 677 (1999).
[3] M. Warner and E. M. Terentjev, *Liquid Crystal Elastomers* (Oxford University Press, Oxford, 2003).
[4] H. Finkelmann, E. Nishikawa, G. G. Pereira, and M. Warner, Phys. Rev. Lett. **87**, 015501 (2001).
[5] P. M. Hogan, A. R. Tajbakhsh, and E. M. Terentjev, Phys. Rev. E **65**, 041720 (2002).
[6] M. Warner and E. M. Terentjev, Macromol. Symp. **200**, 81 (2003).
[7] Y. L. Yu, M. Nakano, and T. Ikeda, Nature (London) **425**, 145 (2003).
[8] Y. L. Yu, M. Nakano, and T. Ikeda, Pure Appl. Chem. **76**, 1467 (2004).
[9] M. Kondo, Y. L. Yu, and T. Ikeda, Angew. Chem., Int. Ed. **45**, 1378 (2006).
[10] M. Camacho-Lopez, H. Finkelmann, P. Palffy-Muhoray, and M. Shelley, Nat. Mater. **3**, 307 (2004).
[11] M. Warner and L. Mahadevan, Phys. Rev. Lett. **92**, 134302 (2004).
[12] P. Rochon, E. Batalla, and A. Natansohn, Appl. Phys. Lett. **66**, 136 (1995).
[13] D. Y. Kim, L. Li, X. L. Jiang, V. Shivshankar, J. Kumar, and S. K. Tripathy, Macromolecules **28**, 8835 (1995).
[14] N. K. Viswanathan, D. Y. Kim, S. Bian, J. Williams, W. Liu, L. Li, L. Samuelson, J. Kumar, and S. K. Tripathy, J. Mater. Chem. **9**, 1941 (1999).
[15] Z. Y. Wei and L. H. He, J. Chem. Phys. **124**, 064708 (2006).
[16] P. G. de Gennes, in *Liquid Crystals of One- and Two-Dimensional Order*, edited by W. Helfrich and G. Heppke (Springer, Berlin, 1980), p. 231.
[17] H. R. Brand, H. Pleiner, and P. Martinoty, Soft Mater. **2**, 182 (2006).
[18] I. S. Gradshteyn and L. M. Ryzhik, *Table of Integrals, Series, and Products* (Elsevier, Singapore, 2004).
[19] A. M. Mathai, *A Handbook of Generalized Special Functions for Statistical and Physical Sciences* (Oxford University Press, New York, 1993).
[20] D. Corbett and M. Warner, Phys. Rev. Lett. **96**, 237802 (2006).